Solid State Communications 173 (2013) 24–29

Contents lists available at ScienceDirect

Solid State Communications

journal homepage: www.elsevier.com/locate/ssc

Graphene nanoribbon intercalated with hexagonal boron nitride: Electronic transport properties from *ab initio* calculations

José Eduardo Padilha [a], Renato Borges Pontes [b], Antônio José Roque da Silva [a,c], Adalberto Fazzio [a,*]

[a] Instituto de Física, Universidade de São Paulo, CP 66318, 05315-970 São Paulo, SP, Brazil
[b] Instituto de Física, Universidade Federal de Goiás, CP 131, 74001-970 Goiânia, GO, Brazil
[c] Laboratório Nacional de Luz Síncrotron, CP 6192, 13083-970 Campinas, SP, Brazil

ARTICLE INFO

Article history:
Received 15 April 2013
Received in revised form
17 June 2013
Accepted 23 August 2013
by Umesh Waghmare
Available online 5 September 2013

Keywords:
A. Graphene nanoribbons
A. Hexagonal boron nitride
D. Magnetic tunnel junction
E. DFT+NEGF transport calculations

ABSTRACT

A magnetic tunnel junction consisting of a boron nitride nanoribbon contacted by two semi-infinite electrodes composed of (3,0) ferromagnetic zig-zag graphene nanoribbons was investigated. Performing spin-polarized *ab initio* transport calculations based on a scheme that combines non-equilibrium Green's function with density functional theory (NEGF+DFT) we predict that such system could act as spin-filter (the efficiency reaches 50%) and present a magnetoristance of 10^5%, depending on the length of the boron nitride region.

1. Introduction

A single layer of graphite, named graphene, received the attention of the condensed matter physics community since its first isolation due to its fascinating properties [1–3]. The collective behavior of electrons added to a honeycomb atomic structure makes graphene a singular material with strong potential for technological applications. Due to a small spin-orbit coupling and a long spin relaxation length [1,2,4–7], graphene and its derivatives as well as other 2D structures, like silicene, have also attracted a great deal of the attention for applications in spintronic devices, such as spin-valves and spin-filters [8–16]. Experimentally, it has been shown that graphene-based spin-valves present a very small magnetoresistance, around 10% at 300 K [9] and 12% at 7 K [10]. One way to increase such value is to use graphene nanoribbons, since they can present a magnetic moment at the edges. Some theoretical studies have predicted very large values of magnetoresistance for such systems [17–19].

Distinct from graphene, the hexagonal boron nitride (h-BN), which also has a honeycomb crystal lattice, is an insulator with a large bandgap (approximately 4.5 eV) [20]. The nanoribbons based on h-BN do not present a magnetic moment at the edges, except under an external perturbation or edge modifications [21–23]. Motivated by recent experimental realizations that synthesized structures composed of graphene and hexagonal boron nitride [24,25], some theoretical works have investigated systems composed of boron nitride nanoribbons (BNNR) and graphene nanoribbons (GNR) connected in parallel [26–29]. Moreover, a recent work treated heterostructures composed of BNNR and GNR connected in series, where the authors explored the transport properties of a two probe and a three terminal field effect transistors (FET) [30]. Nevertheless, little has been done for this system on the spirit of spintronics devices, and some questions still needed to be addressed, for example: What would be the behavior of the transport properties of a magnetic system (GNR) connected with a non-magnetic insulator (BNNR)? Could this system be viewed as a magnetic tunnel junction? All these questions have to be considered if we intend to use such systems as active elements in spintronics devices.

In this paper, we investigate a magnetic tunnel junction consisting of a hexagonal boron nitride nanoribbon contacted with two semi-infinite leads composed of (3,0) ferromagnetic zig-zag graphene nanoribbons. Performing *ab initio* transport calculation we predict that such system could act as spin-filter (the efficiency reaches 50%) and also can present an intrinsic magnetoresistance of 10^5%.

2. Computational methods

The magnetic tunnel junctions (MTJ) are promising candidates for applications in modern magnetic devices [31,32]. These junctions are

* Corresponding author. Tel.: +55 11 3091 70 39.
E-mail addresses: padilha@if.usp.br (J.E. Padilha), pontes@if.ufg.br (R.B. Pontes), ajrsilva@if.usp.br (A.J.R. da Silva), fazzio@if.usp.br (A. Fazzio).

0038-1098/$ - see front matter © 2013 Elsevier Ltd. All rights reserved.
http://dx.doi.org/10.1016/j.ssc.2013.08.022

composed of an insulating material between two ferromagnetic contacts. If the insulating spacer is thin enough, electrons coming from one electrode can tunnel into the other. The current through the insulating material depends on the magnetic moments of the leads, thus there are two important quantities to be determined: (i) the Spin-Filter Efficiency (SFE) defined as $SFE = (I_{up} - I_{down})/(I_{up} + I_{down})$, where $I_{up}(I_{down})$ stands for the current for majority(minority) spin in a measurement with the magnetic moments of the leads in a parallel alignment (P); (ii) The Tunnel Magnetoresistance ratio (TMR) is defined as $TMR = (I_P - I_{AP})/I_{AP}$, where I_P is the current for a parallel alignment of the magnetic moments of the electrodes and I_{AP} is for an anti-parallel alignment [33–35]. The strength of the SFE and TMR is closely related to the spin-polarization of the electrons [36]. In this sense, we can use ferromagnetic graphene nanoribbons (GNR) as contacts and a hexagonal boron nitride ribbon (BNNR) as the non-magnetic insulator.

A ball-and-stick view of the system that we have studied is shown in Fig. 1(a1). They consist of zig-zag hexagonal boron nitride nanoribbons (BNNR) contacted with two semi-infinite ferromagnetic zig-zag graphene nanoribbon electrodes (GNR) [37]. The lengths of the BNNR go from ≈ 2.5 Å to ≈ 16.3 Å corresponding to $N = 1,\ldots,6$ unit cells of BNNR. We consider the (3,0) zig-zag GNR, following Ezawa's notation [38]. The structural and electronic properties were obtained from *ab initio* total energy calculations based on density functional theory [39,40], as implemented in SIESTA code [41]. For the exchange-correlation term we use the GGA-PBE approximation [42]. To describe the interactions of the valence and core electrons we used norm conserved pseudopotentials, as proposed by Troullier–Martins [43]. A double-zeta basis set plus a polarization function (DZP) and an energy cutoff of 300 *Ry* were used to expand the Kohn–Sham orbitals and to represent the charge density on the grid, respectively. The structures were considered relaxed when the residual forces on the atoms were smaller than 0.02 eV/Å. The STM images were simulated using the Tersoff–Hamann procedure [44], which is a well established method in the literature [45–53].

The spin-polarized electronic transport calculations were performed based on the Non-Equilibrium Green's Function method combined with DFT (NEGF–DFT) as implemented in the TRANSAMPA code [54,55,58]. In the calculations the total transmission coefficients, $T^{\uparrow,\downarrow}(E,V)$, were calculated self-consistently at finite bias and integrated according to the Landauer–Büttiker scheme to provide the spin-resolved currents given by

$$I^{\uparrow,\downarrow} = \frac{e}{h}\int_{-\infty}^{+\infty} T^{\uparrow,\downarrow}(E,V)[f_L(E,\mu_L) - f_R(E,\mu_R)]\,dE.$$

where e is the electron charge, h is Planck's constant and $f(E,\mu)$ is the Fermi–Dirac function. An applied bias,V, shift the left and right chemical potential as $\mu_{L/R} = E_F \pm eV/2$, with E_F being the pristine zig-zag GNR Fermi energy.

3. Results and discussions

In Fig. 1, we show the STM images for N varying from 1 to 6 unit cells of BNNR with a bias voltage, V_b, of $+0.5$ V. For few uc's of BNNR ($N = 1$–4) it is possible to see that the states coming from the π cloud of the GNR penetrate inside the BNNR. For the considered voltage, as we increase the number of BNNR unit cells, for example, to 5 unit cells, we verify that the BNNR becomes less visible in the STM. One important point to observe is that due to the difference between the chemical potentials of the B and N atoms on the edges of the BNNR the STM images present a non-symmetric pattern, indicating that the BNNR could influence in a different way the states on opposite edges.

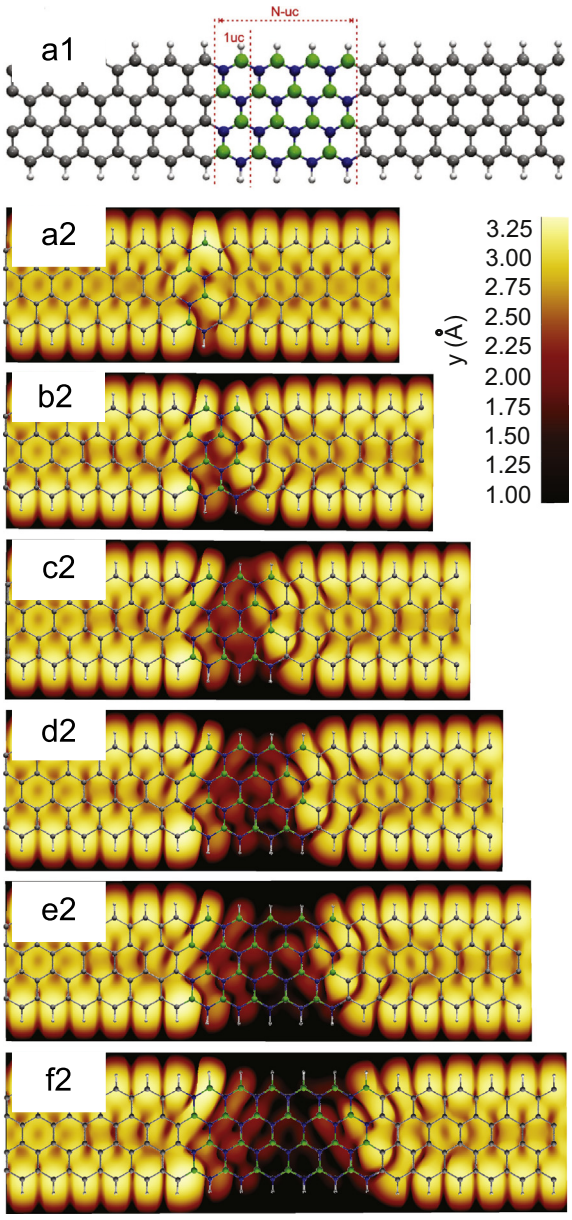

Fig. 1. (Color online) (a1) Schematic representation of the systems used on the calculations. The systems correspond to a central region composed of $N = 1,\ldots,6$ unit cells of a (3,0) zig-zag hexagonal boron nitride nanoribbon intercalated between two (3,0) zig-zag graphene nanoribbons. (a2–f2) Simulated STM images where N is varied between 1 and 6 unit cells of BNNR in the central part of the system. The voltage considered was 0.5 V.

In Fig. 2(a), we show a schematic view of the magnetic order configurations of the leads used on the spin-polarized electronic transport calculations. The magnetic moments between the leads can be aligned in parallel (P) or anti-parallel (AP). In Fig. 2(b) and (c) we show the local magnetization, $\rho_{up} - \rho_{down}$, for a representative system, consisting of a BNNR with ≈ 7.5 Å of length (3 unit cells of BNNR) on a parallel (P) (Fig. 2(b)) and anti-parallel (AP) (Fig. 2(c)) spin configuration of the leads. In the regions close to the BNNR, there was no suppression of the local magnetization on the neighboring GNR. This behavior is distinct from what is obtained for a single impurity of boron or nitrogen doping the nanoribbon [55].

The ground state of zigzag graphene nanoribbons is anti-ferromagnetic (AFM) and, have an electronic bandgap [56]. Due to this fact, the transport properties presented in this paper were calculated considering only ferromagnetic (FM) coupling between

the edges of the GNR. However, it is important to point that, with the application of a transverse electric field, the AFM nano-ribbon becomes half-metallic [57]. We thus believe that it would be possible to obtain transport through the system in the proposed configuration. Moreover, the presence of the BN separating the two ribbons would allow the application of electric fields in different directions. This would allow an on–off control of polarized current via the reversal of the electric field in one of the nanoribbons while the electric field of the other nanoribbon would be kept fixed.

In Fig. 3 we present, for the P conformation of the GNR, the net magnetization as a function of the number of BNNR uc. For 1 unit cell of BNNR, we verify the existence of magnetization at the edges, even in the BNNR part, which is induced by the GNR magnetization. Also, there is a small local magnetization in the interface region between the GNR and the BNNR. Increasing the number of BNNR unit cells we can clearly note a drop of the net magnetization in the BNNR region, showing that we are, in fact, dealing with a ferromagnetic system connected with a nonmagnetic insulating material. Moreover, it is interesting to note the asymmetrical behavior of the net magnetization at the interface regions. This happens because the interface regions (left and right) are asymmetrical regarding the number of BN pairs: in one side there are two BN pairs (left side) and in the other side there is only one BN pair (right side).

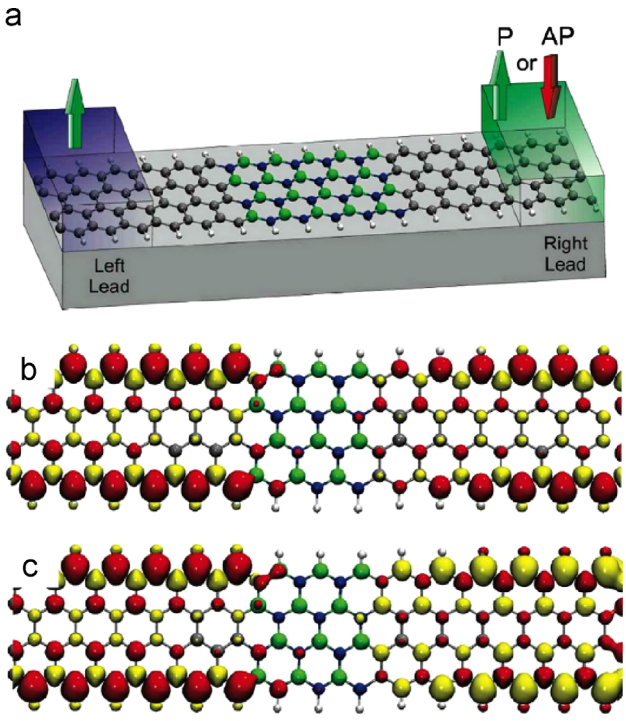

Fig. 2. (Color online) (a) Schematic view of the magnetic configurations of the electrodes used on the transport calculations. The spin directions which are indicated by the arrows can be controlled by an external magnetic field. P (green arrow) indicates the parallel spin alignment of the left and right leads and AP (red arrow) indicates the anti-parallel spin alignment of the leads. (b), (c) Local magnetization, $\rho_{up}-\rho_{down}$, of the systems. The colors red and yellow are associated with spins up and down, respectively. The isosurface value used was 0.001 e/bohr^3.

In Fig. 4, we show the calculated electronic transport properties, in the absence of a bias potential (linear regime), for $N=1$–6 unit cells of BNNR. We can note that as the number of BNNR unit cells increases, there is a decrease in the value of transmittance in the whole energy range considered. Moreover, a large spin polarization on the transmittance is created, mainly on the bulk states of the system, which are located near the Fermi level (-0.4 eV and $+0.4$ eV). For the pristine case, in this energy range, the transport is completely degenerated with respect to spin as shown in Fig. 3(a) (dashed lines). However, we can see that even for 6 layers of BNNR, the transmission coefficient of the system never goes to zero, and the system always presents a spin polarization, as can be seen in panel (g) of Fig. 3. This is a clear evidence of the presence of an electronic tunneling through the insulating BNNR barrier. Another point, in Fig. 3(g), for 2, 3, and 4 uc the transmission function at the Fermi level is higher for the down channel, and this behavior will be reflected on the current flowing through the system as we will see later on.

Before we get into the results for the tunnel junction under an external bias potential, we present some results for pristine (3,0) zig-zag graphene nanoribbon. The main goal of this calculation is to define an energy range to apply the bias voltage which isolates the edge effect. We considered the parallel alignment of the spins in both leads. In Fig. 5(a), we show a plot of $I \times V_{ds}$ curve, for the P spin alignment of the leads. In Fig. 5(b), we show the spin-filter efficiency, SFE, which is given by

$$SFE[\%] = 100\% \times \frac{I_{up}-I_{down}}{I_{up}+I_{down}}.$$

Below a bias voltage of 0.3 V the current is spin degenerated, in agreement with other works [55]. Above this value, the up and down currents are no longer degenerate and this occurs due to an asymmetry between the up and down edge states and to the

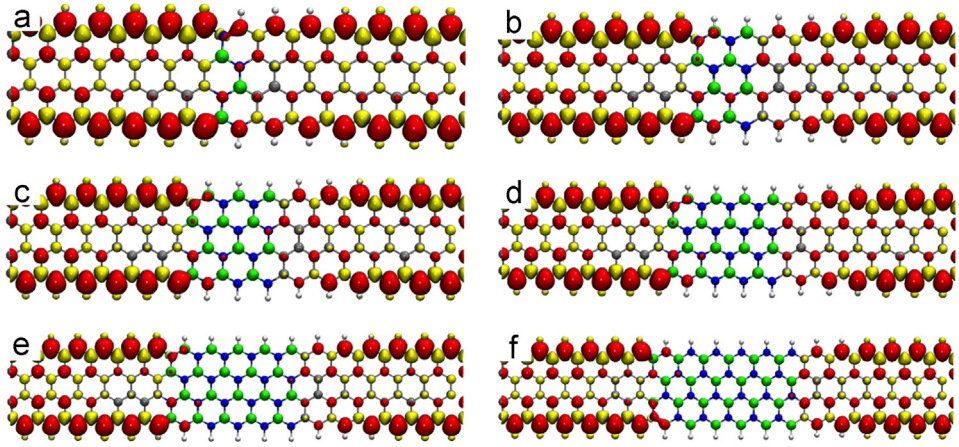

Fig. 3. (Color online) (a–f) Local magnetization, $\rho_{up}-\rho_{down}$, of the studied systems. The colors red and yellow are associated with spins up and down, respectively. The isosurface value used was 0.001 e/bohr^3.

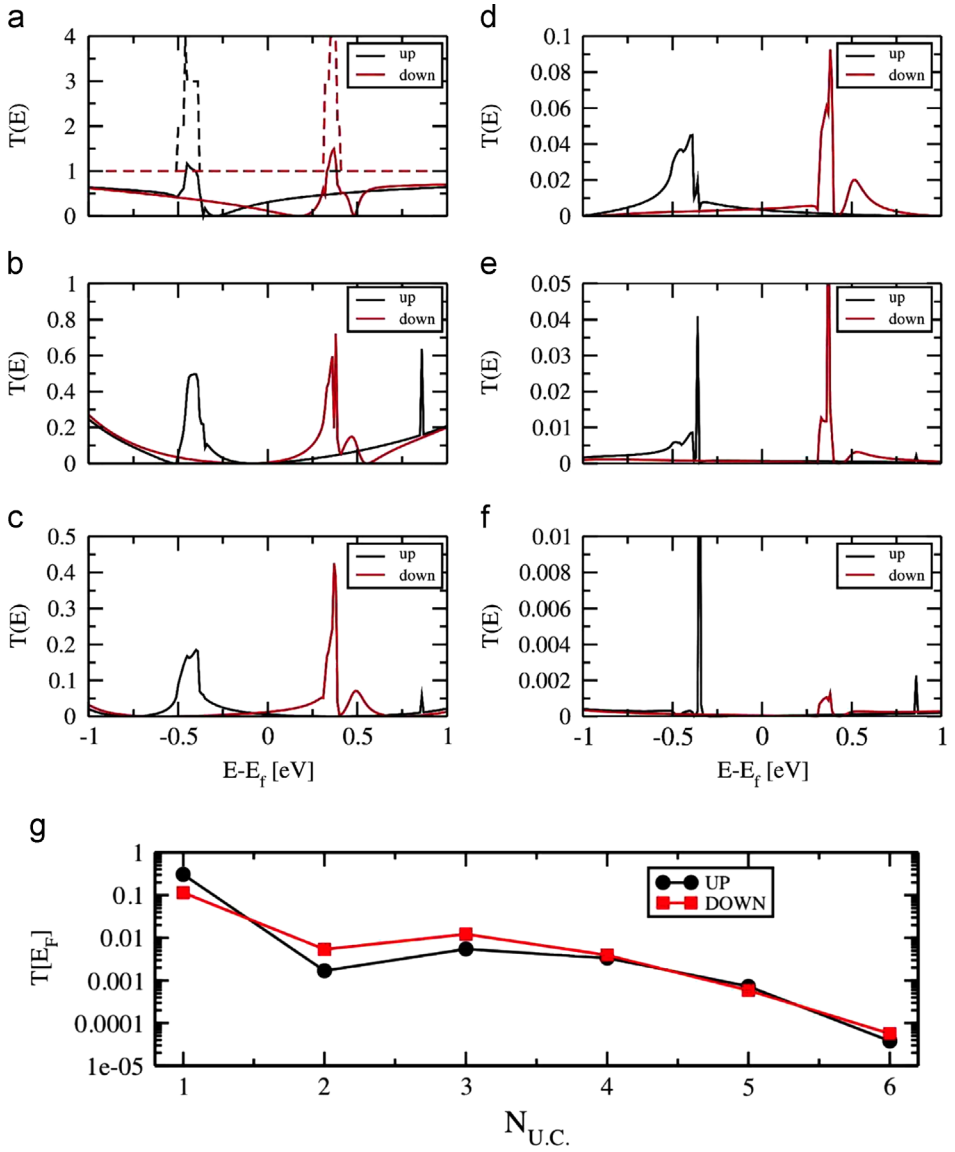

Fig. 4. (Color online) Transmission coefficient [$T(E)$] of the systems composed of (a) 1, (b) 2, (c) 3, (d) 4, (e) 5 and (f) 6 unit cells of BNNR. In panel (g) we present the transmission coefficient, at the Fermi level, as a function of the number of the unit cell (N_{uc}). The dashed lines in (a) corresponds to the transmittance of a pristine GNR.

misalignment of these states as a function of the applied bias voltage [55]. Then, as we want to understand what is the intrinsic influence on the current polarization caused by the insulating material, we will confine our investigation to bias voltages smaller than 0.3 V.

In Fig. 6, we present the calculated $I \times V$ curves for all systems considered (shown in Fig. 3). We observe that the behavior of the curves as a function of bias voltage is very similar in all cases. For 1 uc the current is higher for the up channel. However, for this configuration, the overlap between the left and right electrodes of the GNR is still very large, and the system is not in a tunneling regime. The behavior resembles a superposition of a single boron/nitrogen impurity on each side of the scattering region [55]. For 2, 3 and 4 uc of BNNR [Fig. 6(b, c and d)], respectively, the current is higher for the down channels. This happens because the resonances for the down channel are closer to the Fermi level and, therefore, its exponential tail is larger within the transport window. This behavior can be seen in Fig. 4(g), where the transmittances at the Fermi level are always higher for the down channel. For 5 and 6 uc of BNNR [Fig. 6(e and f), respectively], the currents are almost degenerate for both spin channels. In addition, even if the current falls down by several orders of magnitude, from μA to nA, there is always a current flowing through the system, even for a very low bias voltage of 0.01 V, characteristic of a tunneling regime.

In Fig. 7(a,b), we show the results for the spin-filter efficiency as a function of the length of BNNR. For these calculations we considered a small bias voltage of 0.01 V. We note that depending on the length of BNNR, we can obtain a current that is either higher for majority spins or higher for the minority spins. The values of SFE oscillates around 50% for both the parallel and anti-parallel case, for example for $L \approx 2.5$ Å (1 uc) $SFE \approx 50\%$ and, for $L \approx 5$ Å (2 uc) $SFE \approx -50\%$. One important point to be noted is that increasing the length of the BNNR the value of SFE tends to decrease; thus the device acting as a spin filter will lose functionality with the increase in the number of unit cells of the insulator material.

Another important point to address is the tunnel magnetoresistance (TMR) defined as

$$TMR[\%] = 100\% \times \frac{I_P - I_{AP}}{I_{AP}},$$

where I_P stands for the current for the parallel spin alignment of the leads and I_{AP} is the current for the anti-parallel case.

In Fig. 7(c) we show the TMR as a function of the length of the BNNR. In contrast to the spin-filter efficiency, which has a value of almost zero for $L_{BN} \approx 10$ Å, the TMR reaches its highest value, approximately 10^5%, presenting a giant magnetoresistance.

We have also performed calculations for a (5,0) zig-zag heterostructure (GNR–BNNR–GNR), and similar electron transport behaviors were obtained, which suggest that the performance of these devices has little dependence on the nanoribbon width.

4. Conclusions

In conclusion, motivated by recent experimental realizations, we show based on spin-polarized first-principles calculations that the system composed of a zig-zag hexagonal boron nitride nanoribbon contacted by two zig-zag graphene nanoribbons can

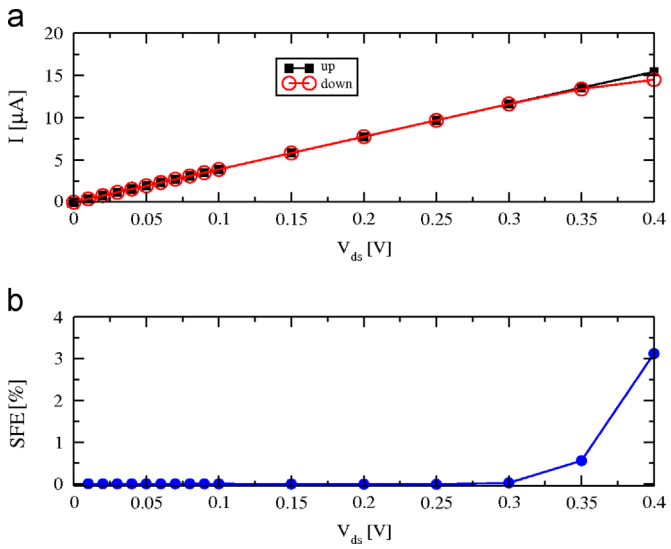

Fig. 5. (Color online) (a) Current–voltage (I –V) characteristics for the pristine graphene nanoribbon. (b) Spin-filter efficiency for the pristine GNR as a function of the bias voltage.

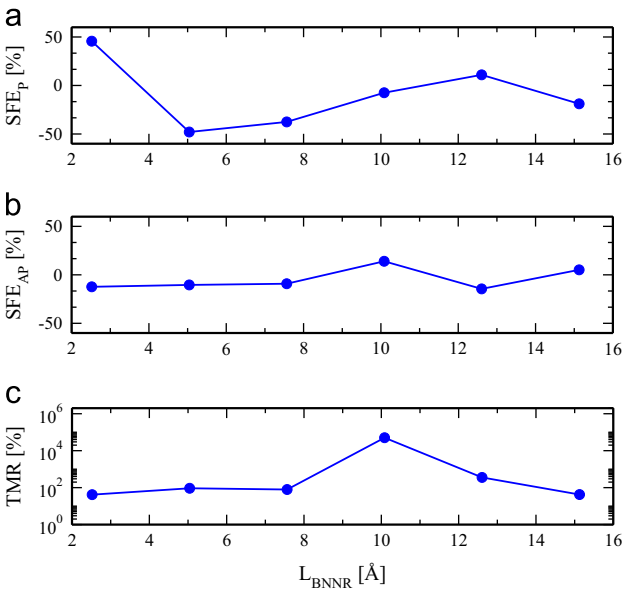

Fig. 7. (Color online) Spin-filter efficiency for the systems with: (a) parallel spin alignment and (b) anti-parallel spins of the electrodes as a function of the length of BNNR. (c) Tunnel magnetoresistance as a function of the length of BNNR.

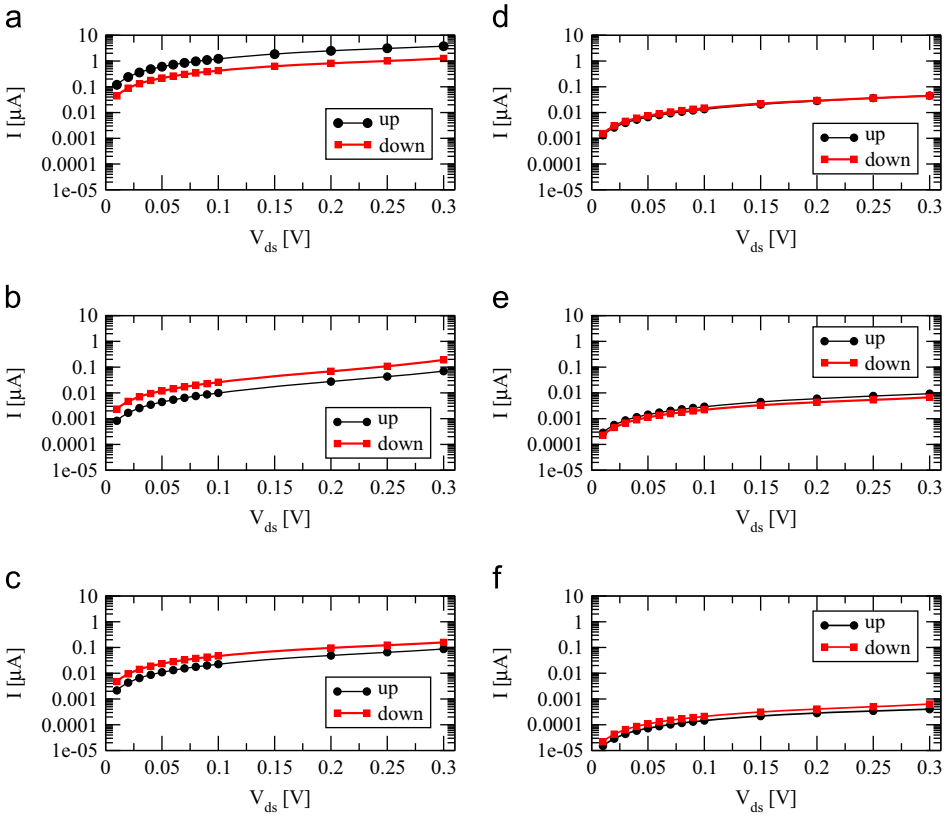

Fig. 6. (Color online) (a)–(f) Spin-polarized plots of the current (I) as a function of the voltage (V_{ds}) for the investigated systems. The number of unit cells was varied from 1 to 6.

be seen as a magnetic tunnel junction. This system could be used either as a spin filter or a device that presents giant magnetoresistance. We also show that such systems could present a spin-filter efficiency of 50% and a magnetoresistance of 10^5%, and this behavior strongly depends on the length of BNNR.

Acknowledgments

The authors thank the Brazilian agencies CAPES, FAPESP and INCT-Nanocarbono/CNPq for financial support. We also thank the CENAPAD-SP for the computational time.

References

[1] K.S. Novoselov, A.K. Geim, S.V. Morozov, D. Jiang, Y. Zhang, S.V. Dubonos, I. V. Grigorieva, A.A. Firsov, Science 306 (2004) 666.
[2] K.S. Novoselov, A.K. Geim, S.V. Morozov, D. Jiang, M.I. Katsnelson, I. V. Grigorieva, S.V. Dubonos, A.A. Firsov, Nature 438 (2005) 197–200.
[3] A.H. Castro Neto, F. Guinea, N.M.R. Peres, K.S. Novoselov, A.K. Geim, Review of Modern Physics 81 (2009) 109–162.
[4] C. Berger, Z.M. Song, T.B. Li, X.B. Li, A.Y. Ogbazghi, R. Feng, Z.T. Dai, A. N. Marchenkov, E.H. Conrad, P.N. First, W.A. de Heer, Journal of Physical Chemistry B 108 (2004) 19912.
[5] C. Berger, Z.M. Song, X.B. Li, X.S. Wu, N. Brown, C. Naud, D. Mayou, T.B. Li, J. Hass, A.N. Marchenkov, E.H. Conrad, P.N. First, W.A. de Heer, Science 312 (2006) 1191.
[6] A.K. Geim, K.S. Novoselov, Nature Materials 6 (2007) 183.
[7] K.S. Novoselov, S.V. Morozov, T.M.G. Mohinddin, L.A. Ponomarenko, D.C. Elias, R. Yang, I.I. Barbolina, P. Blake, T.J. Booth, D. Jiang, J. Giesbers, E.W. Hill, A. K. Geim, Physica Status Solidi B 244 (2007) 4106.
[8] V.M. Karpan, G. Giovannetti, P.A. Khomyakov, M. Talanana, A.A. Starikov, M. Zwierzycki, J. van den Brink, G. Brocks, P.J. Kelly, Physical Review Letters 99 (2007) 176602.
[9] E.W. Hill, A.K. Geim, K. Novoselov, F. Schedin, P. Blake, IEEE Transactions on Magnetics 42 (2006) 2694.
[10] W.H. Wang, K. Pi, Y. Li, Y. Chiang, P. Wei, J. Shi, R. Kawakami, Physical Review B 77 (2008) 020402.
[11] Y.W. Son, M.L. Cohen, S.G. Louie, Nature (London) 444 (2006) 347.
[12] W. Sheng, Z.Y. Ning, Z.Q. Yang, H. Guo, Nanotechnology 21 (2010) 385201.
[13] A. Saffarzadeh, R. Farghadan, Applied Physics Letters 98 (2011) 023106.
[14] A. Avsar, T.-Y. Yang, S. Bae, J. Balakrishnan, F. Volmer, M. Jaiswal, Z. Yi, S.R. Ali, G. GŸntherodt, B.H. Hong, B. Beschoten, B. Özyilmaz, Nano Letters 11 (6) (2011) 2363–2368.
[15] Simon Mutien-Marie Dubois, Xavier Declerck, J.-C. Charlier, Michael C. Payne, ACS Nano 7 (5) (2013) 4578.
[16] W.-F. Tsai, C.-Y. Huang, T.-R. Chang, H. Lin, H.-T. Jeng, A. Bansil, Nature Communications 4 (2013) 1500.
[17] W.Y. Kim, K.S. Kim, Nature Nanotechnology 3 (2008) 408.
[18] R. Qin, J. Lu, L. Lai, J. Zhou, H. Li, Q.H. Liu, G.F. Luo, L.N. Zhao, Z.X. Gao, W.N. Mei, G. Li, Physical Review B 102 (2009) 1368.
[19] F. Muñoz-Rojas, J. Fernández-Rossier, J.J. Palacios, Physical Review Letters 102 (2009) 136810.
[20] K. Watanabe, T. Taniguchi, H. Kanda, Nature Materials 3 (2004) 404.
[21] V. Barone, J.E. Peralta, Nano Letters 8 (2008) 2210.
[22] F. Zheng, G. Zhou, Z. Liu, J. Wu, W. Duan, B.-L. Gu, S.B. Zhang, Physical Review B 78 (2008) 205415.
[23] Y. Wang, Y. Ding, J. Ni, Applied Physics Letters 99 (2011) 053123.
[24] L. Ci, L. Song, C. Jin, D. Jariwala, D. Wu, Y. Li, A. Srivastava, Z.F. Wang, K. Storr, L. Balicas, F. Liu, P.M. Ajayan, Nature Materials 9 (2012) 430.
[25] Z. Liu, L. Ma, G. Shi, W. Zhou, Y. Gong, S. Lei, X. Yang, J. Zhang, J. Yu, K.P. Hackenberg, A. Babakhani, J.-C. Idrobo, R. Vajtai, J. Lou, P.M. Ajayan, Nature Nanotechnology 8 (2013) 119.
[26] E.A. Basheer, P. Parida, S.K. Pati, New Journal of Physics 13 (2011) 053008.
[27] G. Seol, J. Guo, Applied Physics Letters 98 (2011) 143107.
[28] Y.L. Liu, X.J. Wu, Y. Zhao, X.C. Zeng, J.L. Yang, Journal of Physical Chemistry C 115 (2011) 9442.
[29] C. Tang, L.Z. Kou, C.F. Chen, Chemical Physics Letters 523 (2012) 98.
[30] J.C. Dong, H. Li, Journal of Physical Chemistry C (2012), http://dx.doi.org/10.1021/jp304189w.
[31] S. Parkin, Xin Jiang, C. Kaiser, A. Panchula, K. Roche, M. Samant, Proceedings of IEEE 91 (2003) 661.
[32] S.S.P. Parkin, C. Kaiser, A. Panchula, P.M. Rice, B. Hughes, M. Samant, S.-H. Yang, Nature Materials 3 (2004) 862.
[33] M. Julliere, Physics Letters A 54 (1975) 225.
[34] J.S. Moodera, L.R. Kinder, T.M. Wong, R. Meservey, Physical Review Letters 74 (1995) 3273.
[35] T. Miyazaki, N. Tezuka, Journal of Magnetism and Magnetic Materials 139 (1995) L231.
[36] R. Meservey, P.M. Tedrow, Physics Reports 238 (1994) 173.
[37] Although the ferromagnetic configuration between the edges of the graphene nanoribbons (GNR) is not the lowest energy conformation (the total energy difference is on the order of a few eV), we choose this magnetic ordering for the electrodes, since in this configuration the system is metallic.
[38] M. Ezawa, Physical Review B 73 (2006) 045432.
[39] P. Hohenberg, W. Kohn, Physical Review 136 (1964) B864.
[40] W. Kohn, L.J. Sham, Physical Review 140 (1965) A1133.
[41] J.M. Soler, E. Artacho, J.D. Gale, A. García, J. Junquera, P. Ordejòn, D. Sánchez-Portal, Journal of Physics: Condensed Matter 14 (2002) 2745.
[42] J.P. Perdew, K. Burke, M. Ernzerhof, Physical Review Letters 77 (1996) 3862.
[43] N. Troullier, J.L. Martins, Physical Review B 43 (1991) 1993.
[44] J. Tersoff, D.R. Hamann, Physical Review B 31 (1985) 805.
[45] Y. Fujimoto, S. Saito, Physical Review B 84 (2011) 245446.
[46] S.-O. Guillaume, B. Zheng, J.-C. Charlier, L. Henrard, Physical Review B 85 (2012) 035444.
[47] H. Okada, Y. Fujimoto, K. Endo, K. Hirose, Y. Mori, Physical Review B 63 (2001) 195324.
[48] Y. Fujimoto, H. Okada, K. Endo, T. Ono, S. Tsukamoto, K. Hirose, Materials Transactions 42 (2001) 2247.
[49] S. Berber, A. Oshiyama, Physical Review B 77 (2008) 165405.
[50] H. Amara, S. Latil, V. Meunier, Ph. Lambin, J.-C. Charlier, Physical Review B 76 (2007) 115423.
[51] A.A. El-Barbary, R.H. Telling, C.P. Ewels, M.I. Heggie, P.R. Briddon, Physical Review B 68 (2003) 144107.
[52] B. Zheng, P. Hermet, L. Henrard, ACS Nano 4 (2010) 4165.
[53] L. Zhao, R. He, K.T. Rim, T. Schiros, K.S. Kim, H. Zhou, C. Gutiérrez, S. P. Chockalingam, Carlos J Arguello, Lucia Pálová, D. Nordlund, M. S. Hybertsen, D.R. Reichman, T.F. Heinz, P. Kim, A. Pinczuk, G.W. Flynn, A. N. Pasupathy, Science 333 (2011) 999.
[54] F.D. Novaes, A.J.R. da Silva, A. Fazzio, Brazilian Journal of Physics 36 (2001) 799.
[55] J.E. Padilha, R.B. Pontes, A.J.R. da Silva, A. Fazzio, International Journal of Quantum Chemistry 111 (2011) 1379.
[56] M. Fujita, K. Wakabayashi, K. Nakada, K. Kusakabe, Journal of the Physical Society of Japan 65 (1996) 1920–1923.
[57] Y.-W. Son, M.L. Cohen, S.G. Louie, Nature 444 (2006) 347.
[58] J.E. Padilha, M.P. Lima, A.J.R. da Silva, A. Fazzio, Physical Review B 84 (2011) 113412.